https://doi.org/10.17221/100/2020-VETMED

# Preparation of artificial vascularised tissue and the indirect determination of its void volume using µCT

*Christian Seiler[1]*, Matthias Luepke[1], Jan-Peter Bach[2], Hermann Seifert[1]*

*[1]Institute of General Radiology and Medical Physics, University of Veterinary Medicine Foundation, Hannover, Germany*

*[2]Small Animal Clinic, University of Veterinary Medicine Foundation, Hannover, Germany*

**Corresponding author: christianseiler86@yahoo.de*

**Citation:** Seiler C, Luepke M, Bach JP, Seifert H (2022): Preparation of artificial vascularised tissue and the indirect determination of its void volume using µCT. Vet Med-Czech 67, 387–394.

**Abstract:** The non-invasive determination of the vasculature volume would be very useful in many fields of medicine such as oncology and implantation. The purpose of this research was, therefore, to develop a methodology to investigate vascularisation in phantoms using microcomputed tomography (µCT) without having to visualise the single vessels. Epoxy resin and cotton candy were used to form the phantoms with microchannels. The size of the channels was measured via microscopy and the proportion of the void volume (PVV) was calculated. The phantoms were placed in contrast agent solutions of different concentrations and scanned in µCT. The mean CT numbers of the phantoms were calculated with the Amira software and displayed as a function of the determined PVV and the contrast agent concentration (CAC). The fabricated microchannels had the size of biological capillaries (diameter: 5 µm to 15 µm) and the phantoms showed a microchannel density of 5 to15 microchannels per mm². With an increasing CAC, the CT numbers increased significantly. Additionally, the phantoms with a higher PVV also had a higher CT number. The CT numbers and the PVV correlated moderately together, but significantly. The slope of the regression line increased with an increasing CAC.

**Keywords:** capillary phantoms; contrast enhanced; epoxy resin; imaging

Many implantation complications are due to a lack of micro-vascularisation (Santos and Reis 2010). Particularly when using previtalised implants, a quick supply of attached cells is important (Cassell et al. 2002; Nomi et al. 2002; Malda et al. 2007), as otherwise they could die off (McMurtrey 2016). In order to sufficiently supply these cells with oxygen and nutrients, the rapid formation of blood vessels is essential, as the average diffusion depth of these substances only reaches 100–200 µm in the extracellular medium (Cassell et al. 2002; Rouwkema et al. 2010). However, most clinical imaging techniques, such as computed tomography (CT), are not capable of dissolving these fine, few microns thick capillaries (Schmidt et al. 2010; Pal 2017).

In order to investigate the progress of vascularisation in animals, the implant is either examined through intravital fluorescence microscopy or removed at different times and examined histologically. However, both methods require highly invasive surgical interventions, which often lead to the death of many laboratory animals. Therefore, this study attempts to develop an *in vivo* (artificial simulated) and non-invasive method to indirectly determine the vascularisation in tissue, i.e., without directly dissolving the individual capillaries using imaging techniques.

In order to simulate freshly vascularised tissue, phantoms with microchannels the size of capillaries were created (Bellan et al. 2009). These phantoms were scanned in different contrast agent

https://doi.org/10.17221/100/2020-VETMED

concentrations (CACs) in a micro-CT (μCT), whose spatial resolution was considerably higher than the microchannel size. The microchannel volume should only be estimated from the radiodensity [stated as the CT-number in Hounsfield Units (HU)] of the examined volume at different CACs. The possibility of evaluating the micro-vascularisation *in vivo* would reduce the necessity for laboratory animals in sequential studies like is required in the Basel Declaration in the 3R Principle.

## MATERIAL AND METHODS

### Development of the microchannel phantoms

The basic material used for the phantoms was epoxy resin (epoxy resin L 385; R&G Faserverbundwerkstoffe GmbH, Waldenbruch, Germany), as the resin is easy to process and did not show any water absorption in the preliminary studies.

To produce microchannels, spun sugar fibres were used from a commercially available cotton candy machine (ZWM 3478; Clatronic International GmbH, Kempen, Germany). A thin layer was removed from the spun cotton candy and placed on a cured resin layer (base layer). Thick threads approximately 0.5 mm to 2 mm in size were pulled from the heated viscous sugar mass and laid in squares over the thin cotton candy layer to ensure connection to the microchannels. Thereby, the resin-sugar construct was divided into small fields of different sizes. This sugar network was then doused with a second layer of epoxy resin and degassed. The resin casting steps took place in a rectangular plastic box and the phantom was removed after curing.

The resin-sugar construct was then placed in a bigger mould filled with distilled water and stored in a heated ultrasonic bath until the sugar network in the resin was completely dissolved and fine microchannels were formed in addition to the large main channels. The resulting microchannel phantoms consisted only of the epoxy resin and were divided by the main channels into small fields with microchannels (Figure 1). Two phantoms with dimensions of 80 mm × 110 mm were made this way. One with 12 fields (Figure 1) and one with 14 fields. The total thickness of the phantoms is about 9 mm, of which about 5.6 mm is the base layer and the microchannels are in a 3.4 mm thick layer only.

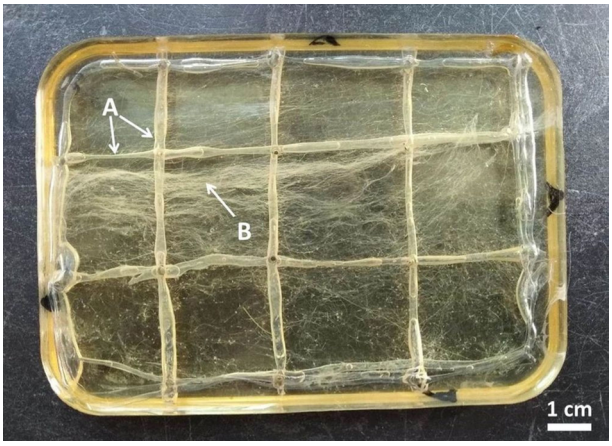


Figure 1. Top view of one of the two microchannel phantoms with the main channels – A and microchannels – B within its 12 fields

### Analysis of the microchannel volume

To measure the diameter of the microchannels, the phantoms were crushed and the top layer of randomly selected pieces was carefully ground off so that the diameter of the microchannels could be measured with a light microscope (KF2; Carl Zeiss Jena GmbH, Jena, Germany) at 400-fold magnification with a calibrated ocular grid. A total of 217 randomly selected microchannels were measured in this way. A representative distribution of the size of the microchannels was determined. In addition, the mean diameter $\overline{d_m}$ and the mean cross-sectional area $\overline{A_m}$ (assuming a circular cross-section) of the microchannels were calculated. To determine the total microchannel volume of a field, digital images (Nex-5T; Sony Inc., Tokyo, Japan) were taken at 20-fold magnification with a reflected light microscope (Stereomicroscope; Phywe System GmbH&Co. KG, Göttingen, Germany) (see Figure 2A). The images were then converted into 8-bit representation using the ImageJ software (NIH, Bethesda, MD, USA) and treated with a bandpass filter to provide uniform background brightness throughout the image (Figure 2B). The microchannels could be separated from the background with the threshold function, and their area and percentage $p_m$ on the image were calculated (Figure 2C). Assuming that the predetermined distribution of the microchannel diameters was the same for all the fields, the void volumes of the microchannels of each field $V_m$ were calculated as follows:

$$V_m = p_m \cdot A_F \cdot \overline{A_m} \Big/ \overline{d_m} \quad (1)$$

https://doi.org/10.17221/100/2020-VETMED

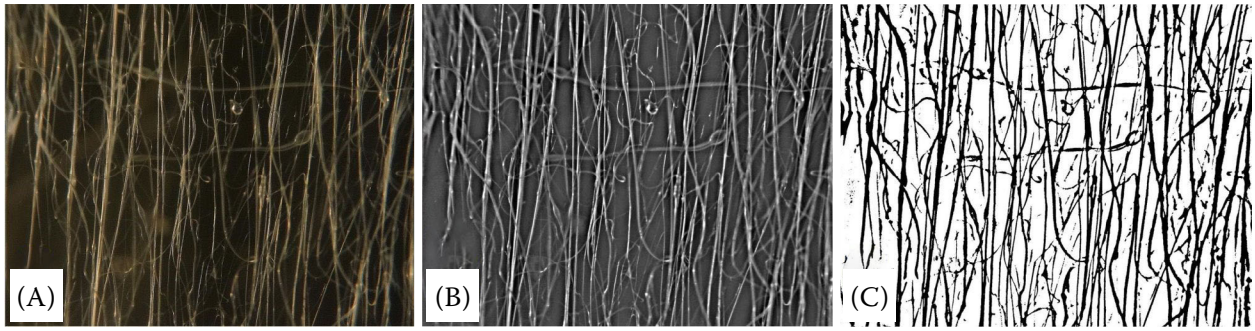


Figure 2. Analysis and evaluation of the microchannel pictures
(A) Digital image of the microchannels under the reflecting microscope at 20-fold magnification. (B) The microchannels could be clearly detached from the background by converting them into an 8-bit image and using a bandpass filter. (C) The threshold function divides the image into black and white and allows the evaluation of the percentage $p_m$ of black in the image

where:

$p_m$ – denotes the percentage of channels in the digital image;

$A_F$ – the area of a field;

$\overline{A_m}$ and $\overline{d_m}$ – the mean values of the circular cross-sectional area and the diameter of the microchannels, respectively.

## µCT scans

The phantoms were placed in contrast agent solutions [Xenetix 350 (Iobitridol); Guerbet GmbH, Sulzbach, Germany] at various concentrations. For this purpose, distilled water was mixed with the contrast agent at a concentration of 0, 3, 6, 9, 12 or 15 ml of contrast agent per litre of water (CAC0, CAC3, CAC6, CAC9, CAC12, CAC15), respectively. To ensure that the contrast medium solution also penetrated into the microchannels, the phantoms were stored for 48 h in the respective solution before scanning. Both phantoms were scanned with all the different CACs. For this purpose, they were rinsed in between with distilled water for 48 h each.

All the scans were performed on an XtremeCT (Scanco Medical AG, Brüttisellen, Switzerland) with a fixed tube voltage of 60 kV. For the spatial resolution and integration time, values of 81 µm and 1 400 ms were selected, respectively.

## Analysis of the µCT scans

All the scans were converted into DICOMs and evaluated with the Amira software (v6.5.0; Thermo Fisher Scientific Inc., Waltham, MA, USA). By means of suitable contrast settings, it was possible to identify and segment the main channels and thereby the individual fields of the phantom. The segmentation of each field was performed manually and oriented on the main channels that were also clearly visible in the µCT images (see Figure 3). For the thickness or depth, we were guided by the resin cover layer, which we could recognise particularly well in the transverse sectional plane in the µCT images. Since the main channels lay directly on the resin base layer, the cover layer extended exactly from the lower end of the main channels to the surface of the phantoms. This created a kind of template for each field, which we could also use with the other

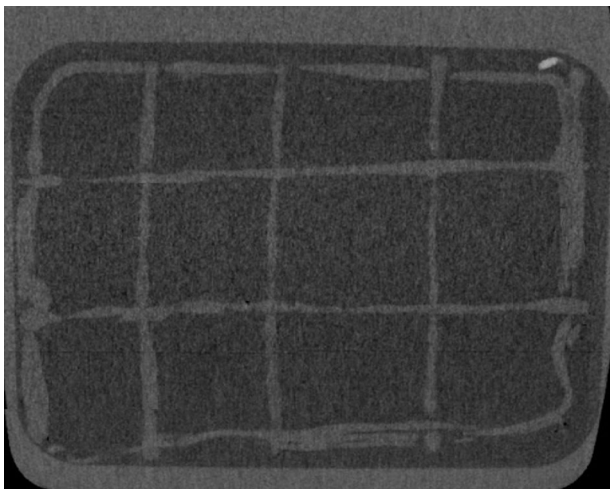

Figure 3. Exemplary µCT image (resolution: 81 µm) of a phantom at a contrast agent concentration of 9 ml per litre of water
The main channels can be seen very well and, thus, also the individual fields

https://doi.org/10.17221/100/2020-VETMED

contrast agent concentrations. Both the volume and the mean CT number of each segmented field were calculated automatically using the Amira software.

### Statistical analysis

The estimated microchannel volume was divided by the segmental volume of the field to determine the percentage of the microchannel volume in the total volume of the field. The measured CT numbers were plotted against the proportion of the void volume (PVV) and against the CAC. The change in the CT numbers of the 26 fields ($N$ = 26) with an increasing contrast agent concentration (CAC) with an analysis of variance (ANOVA) after the CT numbers of the 26 fields were tested on normal distribution (Kolmogorov-Smirnov) at each CAC. As the ANOVA indicated a significant ($P < 0.001$) change, each group was compared to the group with the next highest CAC using a paired $t$-test.

In addition, the 26 fields were divided into 13 fields with a small PVV ($N$ = 13) and 13 fields with a large PVV ($N$ = 13) and the same statistical analysis was performed (Kolmogorov-Smirnov, ANOVA, paired $t$-test). The respective dependency was also tested with a correlation and regression analysis. Subsequently, the differences in the two groups (small PVV – large PVV) at the same CAC were directly calculated with a paired $t$-test.

## RESULTS

### Analysis of the microchannel volume

All the measured microchannels showed a diameter between 0 and 50 µm, with the majority (78%) between 5 and 15 µm. This resulted in an average diameter $d_m$ of 11.1 µm and a cross-sectional area $\overline{A_m}$ of 138 µm². The distribution of the diameters is shown in Figure 4.

The 26 fields of the two phantoms had a microchannel volume between 0.47 and 2.77 mm³ per field with an average of 1.30 mm³. Since the individual fields differed in size, this corresponded to a PVV of 0.07% to 0.21% with an average of 0.14% at a thickness of 3.4 mm. This equalled a microchannel density of approximately 5.0 to 15.1 microchannels per mm², with an average of 10.0 mm$^{-2}$ (formula: PVV × 1 mm²/$\overline{A_m}$).

### Analysis of the µCT scans

The analysis of the 26 fields in the µCT [Figure 5 and Table S1 in electronic supplementary material (ESM); for the supplementary material see the electronic version] showed a significant increase in the CT number with a stepwise increase in the CAC from CAC0 to CAC9. Although the increase in CAC12 or CAC15 also led to an enhancement in the CT number, the change was not significant.

The evaluation of the 13 fields with the smallest PVV (0.07–0.15%) showed an increasing CT number until CAC9 and a minimal decrease thereafter (CAC12 and CAC15). A significant difference was only detected in the increase from CAC0 to CAC3 and CAC6 to CAC9. In the evaluation of the 13 fields with the higher PVV (0.15–0.21%), the CT number always increased significantly from 53.0 HU (CAC0) to 71.8 HU (CAC15); one exception was the change from CAC9 to CAC12. When both groups were

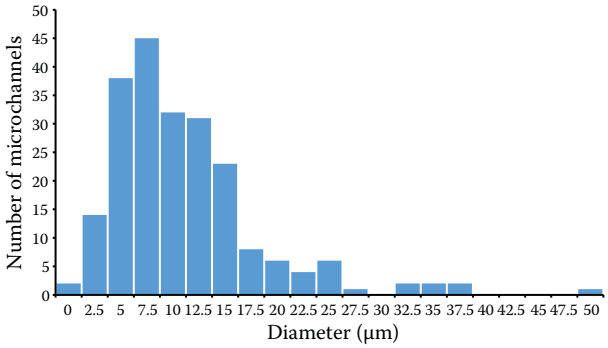


Figure 4. Distribution of the diameters of the 217 measured microchannels

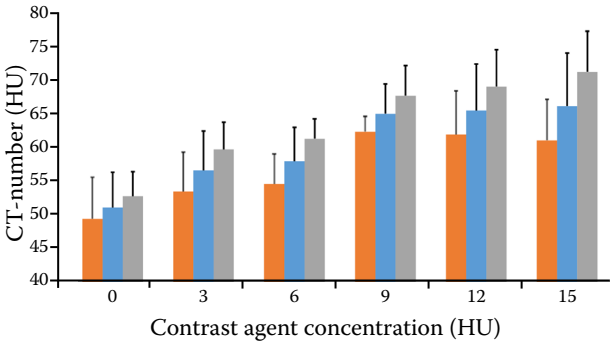


Figure 5. Increase in the CT-numbers of the fields with an increasing contrast agent concentration

The orange bar shows the averaged CT-numbers of the 13 fields with the smallest proportion of the void volume. The grey bar shows the averaged CT-numbers of the 13 fields with the largest proportion of the void volume. The blue bar is the average of all 26 fields

https://doi.org/10.17221/100/2020-VETMED

compared, the CT numbers of the 13 fields with the higher PVV were significantly higher (*t*-test: $P < 0.006$) than the 13 fields with the smaller PVV, with the exception of CAC0 ($P = 0.10$).

The analysis of the correlation between the PVV and CT numbers of each field showed a moderate, but significant, correlation for all the CACs with values of Pearson's correlation coefficient ranging between 0.41 and 0.74.

Figure 6 and supplementary Table S2 in ESM present the results of the linear regression analysis. With an increasing CAC, the slope of the regression

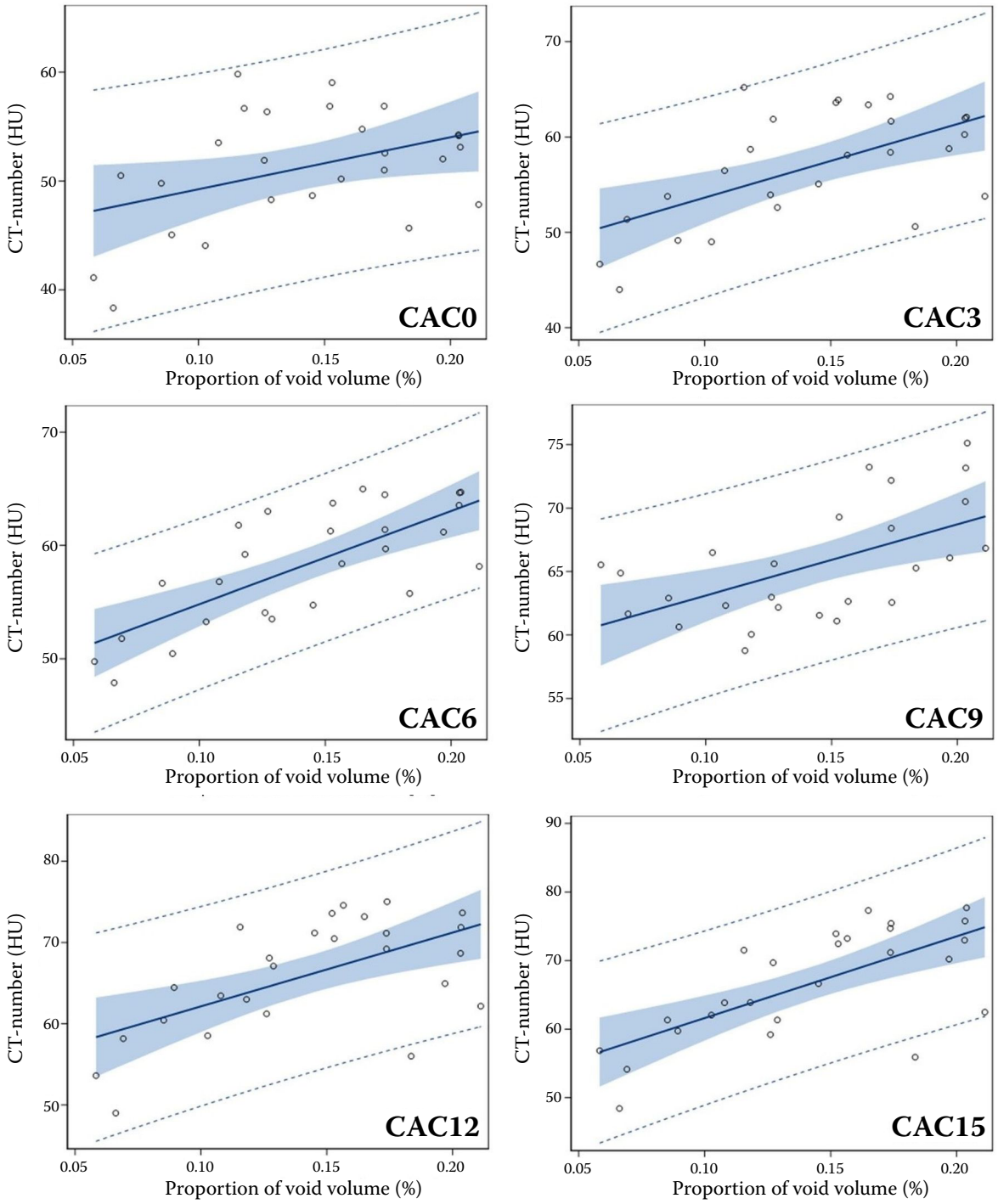


Figure 6. Regression analysis of the proportion of the void volume and the CT-numbers at different contrast agent concentrations

The blue shaded area marks the interval of confidence (95%) and the dotted lines represent the interval of prediction (95%)

https://doi.org/10.17221/100/2020-VETMED

line became steeper from 48 HU/ml/kg (at CAC0) to 119 HU/ml/kg (at CAC15). Only at CAC9, the slope was less steep compared to the slopes at lower CAC. The quality of the fit of the regression lines to the data points (coefficient of determination $R^2$) varied between 0.17 and 0.55 for all the CAC. The values of the intercepts ranged from 44 HU to 57 HU (mean: 50 HU).

## DISCUSSION

One objective of this study was to fabricate phantoms with microchannels with the size of capillaries. The results of the microscopic evaluation showed a very good match between the microchannel diameter (78% in the range of 5–15 µm) with blood capillaries, which are approximately 5–10 µm in size (Schmidt et al. 2010; Pal 2017).

Needless to say, the microscopic analysis of the PVV of the fields is only an approximation to have a rough idea of the extent of the PVV and to be able to sort them according to size. The approximation is based on the presumption that each field has a similar microchannel distribution to the 217 randomly measured channels. The other presumption we have made is that all the channels are circular in diameter, which, of course, does not agree with natural conditions, but is necessary to simplify the approximation.

Deviations from this distribution are natural and cannot be eliminated. However, due to the relatively high number of microchannels in the field, these deviations were kept as low as possible.

To minimise overlapping, we only used a very thin layer of cotton candy to process the phantoms. Therefore, the microchannel network in the resin was almost certainly a two-dimensional network. A minimal underestimation, of course, cannot be precluded for fields with a high PVV.

The phantoms were filled with water with Xenetix350 with a total of 0 ml to 15 ml per kilogram of water. In the information leaflet for Xenetix350, a dose of 1–2.5 ml per kilogram of body weight is suggested for CT scans (Guerbet GmbH 2009). However, since blood – where the contrast agent is mainly distributed in – only amounts to 7% of the body weight, correspondingly higher CACs were used in the study. In addition, in living organisms, the CAC is normally not evenly distributed, but can rise during a bolus, so that much higher CACs will be reached in clinical use than those in our study.

The statistical analysis of the µCT results showed that with an increasing CAC, a significant increase in the CT number was usually detected (Figure 5 and Table S1 in ESM). This implies that the µCT is basically sufficiently sensitive to detect even small changes in the CT number provoked by a contrast injection as would be dispensed in the living organism later. The relatively high standard deviations are caused by averaging over different sized PVVs and, of course, by the natural noise and uncertainty of a µCT scan. These lie in the same scale as the small changes in the CT number and hinder the analysis.

The evaluation of the dependence of the CT number on the PVV of the individual fields showed similar results. There was a correlation between the CT number and the PVV as well as an increment in the slope of the regression line with a higher CAC (Figure 6 and Table S2 in ESM). This is, in principle, the prerequisite for being able to draw quantitative conclusions concerning an increase in the PVV from an increase in the CT numbers. However, the individually measured values also showed considerable variability, so that the differences in CT scores based on a different PVV or CAC were partially masked by the noise of µCT.

A higher PVV or microchannel density has more of an impact on the CT numbers and could reduce the variance in the measurements. In our study, the phantoms had a mean microchannel density of about ten microchannels per mm². This is a rather small number, as previous research in animals and humans showed capillary densities of several hundred capillaries per mm² (c/mm²) (Arieli and Ar 1981; McGuire and Secomb 2003; Egginton 2011). Willems et al. (2012) even measured a capillary ratio of 5–10% in vascularised allogenic bone grafts in rats. Although the capillary densities strongly depend on the particular species and the respective organ, they are always significantly higher than those of self-made phantoms, demonstrating that our microchannel density of only 10 c/mm² is too low even for newly vascularised tissue. An improvement in the manufacturing process that guarantees a higher microchannel density could help to enhance the signal-to-noise ratio.

Modern experimental µCT or nano-CT are even partly able to dissolve capillaries and, thus, used to calculate the capillary volume (Kampschulte et al. 2016; Epah et al. 2018). However, these devices are not yet part of standard equipment in clinical practice.

https://doi.org/10.17221/100/2020-VETMED

Therefore, the purpose of this pilot study was to be able to draw conclusions regarding the PVV of the microchannels whose size was deliberately too small for the spatial resolution of the μCT (82 μm voxel size). Thus, the conclusions should only be based on the differences in the brightness in the CT slice image and on changes in the CT numbers. Later, it should be possible to make quantitative statements about the neovascularisation of, for example, a previtalised implant using a conventional clinical CT whose resolution is in the range of hundreds of micrometres. It remains to be considered that when measuring in real tissue, one can only draw conclusions about the PVV when the CT number changes. It is not possible to say whether the PVV is distributed over large or small capillaries. Either way, a larger PVV always indicates better blood flow. So far, the results of the presented study have not yet allowed such quantitative conclusions to be drawn because of the wide distribution of the measured values.

Nevertheless, they do show that this could be possible if the phantoms are developed further. As mentioned above, this development involves a higher and more diversified microchannel density in the order of 10–500 c/mm². A further innovation should be connecting the phantoms to a hose system including a pump to be able to imitate bolus tracks.

Needless to say, many problems still need to be solved for clinical applications.

For example, the parameters of the μCT still have to be transferred to a clinical CT, and the radiation exposure has to be reduced in order to be able to measure them on living patients in the future. However, these problems are not yet relevant for the current status of the study. The main aim of this pilot study was to show to what extent a quantification of the void volume below the resolution limit is possible, and what improvements need to be made to the study design in order to achieve successful further development.

This pilot study demonstrates a method to produce phantoms with microchannels the size of capillaries using epoxy resin and cotton candy. It also shows that the μCT is basically sufficiently sensitive to estimate the void volume of the microchannels based on the differences in the CT numbers at different contrast agent concentrations. Nevertheless, the noise partially masks these differences, so that further development of phantoms and further measurements are essential to enable clinical applications of this method. The clinical application of such a method could reduce the need for laboratory animals, as required by the 3Rs principle.

## Conflict of interest

The authors declare no conflict of interest.

## REFERENCES

Arieli R, Ar A. Blood capillary density in heart and skeletal muscles of the fossorial mole rat. Physiol Zool. 1981 Jan; 54(1):22-7.

Bellan LM, Singh SP, Henderson PW, Porri TJ, Craighead HG, Spector JA. Fabrication of an artificial 3-dimensional vascular network using sacrificial sugar structures. Soft Matter. 2009 Mar;5(7):1354-7.

Cassell OC, Hofer SO, Morrison WA, Knight KR. Vascularisation of tissue-engineered grafts: The regulation of angiogenesis in reconstructive surgery and in disease states. Br J Plast Surg. 2002 Dec;55(8):603-10.

Egginton S. Physiological factors influencing capillary growth. Acta Physiol (Oxf). 2011 Jul;202(3):225-39.

Epah J, Palfi K, Dienst FL, Malacarne PF, Bremer R, Salamon M, Kumar S, Jo H, Schurmann C, Brandes RP. 3D imaging and quantitative analysis of vascular networks: A comparison of ultramicroscopy and micro-computed tomography. Theranostics. 2018 Mar 7;8(8):2117-33.

Guerbet GmbH. Gebrauchsinformation [Instruction manual of May 2017] [Internet]. 2009 [cited 2018 Mar 21]. Available from: https://www.guerbet.com/media/y3opbwai/fi_xenetix-300_1705.pdf. German.

Kampschulte M, Langheinirch AC, Sender J, Litzlbauer HD, Althohn U, Schwab JD, Alejandre-Lafont E, Martels G, Krombach GA. Nano-computed tomography: Technique and applications. Rofo. 2016 Feb;188(2):146-54.

Malda J, Klein TJ, Upton Z. The roles of hypoxia in the in vitro engineering of tissues. Tissue Eng. 2007 Sep;13(9): 2153-62.

McGuire BJ, Secomb TW. Estimation of capillary density in human skeletal muscle based on maximal oxygen consumption rates. Am J Physiol Heart Circ Physiol. 2003 Dec;285(6):H2382-91.

McMurtrey RJ. Analytic models of oxygen and nutrient diffusion, metabolism dynamics, and architecture optimization in three-dimensional tissue constructs with applications and insights in cerebral organoids. Tissue Eng Part C Methods. 2016 Mar;22(3):221-49.

https://doi.org/10.17221/100/2020-VETMED

Nomi M, Atala A, Coppi PD, Soker S. Principals of neovascularization for tissue engineering. Mol Aspects Med. 2002 Dec;23(6):463-83.

Pal GK. Comprehensive textbook of medical physiology. New Dehli: Jaypee Brothers Medical Publishers; 2017. p. 817-8.

Rouwkema J, Koopman B, Blitterswijk C, Dhert W, Malda J. Supply of nutrients to cells in engineered tissues. Biotechnol Genet Eng Rev. 2010 Jan;26(1):163-78.

Santos MI, Reis RL. Vascularization in bone tissue engineering: Physiology, current strategies, major hurdles and future challenges. Macromol Biosci. 2010 Jan 11;10(1):12-27.

Schmidt RF, Lang F, Heckmann M. Physiologie des Menschen: Mit Pathophysiologie [Physiology of the human being: With pathophysiology]. Heidelberg: Springer-Verlag; 2010. p. 226-9. German.

Willems WF, Larsen M, Friedrich PF, Shogren KL, Bishop AT. Induction of angiogenesis and osteogenesis in surgically revascularized frozen bone allografts by sustained delivery of FGF-2 and VEGF. J Orthop Res. 2012 Oct; 30(10):1556-62.

Received: May 1, 2020
Accepted: February 24, 2022
Published online: May 1, 2022